

Supporting Information

Widespread Occurrence of Large Molecular Methylsiloxanes in Ambient Aerosols

Table of contents

Figures S1 to S11

Methods S1 to S2

Notes S1 to S6

Models S1 to S2

References (1 to 67)

Other Supporting Materials for this manuscript include the following:

Data S1

14 **Method S1. Identification and quantification of methylsiloxanes**

15 The methylsiloxanes and their derivatives were identified and quantified using a method outlined in our
16 previous studies (Yao et al., 2022, 2023). The identification relied primarily on the ratio between the main
17 peak and the isotope peaks at m/z of $\text{main}+1$ and $\text{main}+2$, as demonstrated in Method Section. The
18 identified methylsiloxanes consisted mainly of small cyclic volatile methylsiloxanes (cVMS,
19 $(\text{Si}(\text{CH}_3)_2\text{O})_n$, $\text{D}_3\text{--D}_n$) and their positively charged fragments ($\text{C}_{2n-1}\text{H}_{6n-3}\text{O}_n\text{Si}_n^+$, denoted as $\text{D}_3\text{f--D}_n\text{f}$),
20 which were formed through the loss of one $-\text{CH}_3$ group during ionization (recent research suggests this
21 process occurs in two steps (Worton et al., 2023)). Additionally, the monomer diol dimethylsilanediol
22 (DMSD, $\text{Si}(\text{CH}_3)_2(\text{OH})_2$) and its fragment $((\text{CH}_3)_2(\text{OH})\text{Si}^+$, referred to as DMHS^+) were detected and
23 included in the analysis. Hydroxylated methylsiloxanes ($\text{C}_{2n+1}\text{H}_{6n+4}\text{O}_{n+2}\text{Si}_{n+1}$, $\text{D}_2\text{T}^{\text{OH}}\text{--D}_n\text{T}^{\text{OH}}$) and their
24 corresponding fragments ($\text{C}_{2n}\text{H}_{6n}\text{O}_{n+2}\text{Si}_{n+1}^+$, labeled as $\text{D}_2\text{T}^{\text{OHf}}\text{--D}_n\text{T}^{\text{OHf}}$) were also identified and
25 quantified. For clarity and ease of interpretation, the fragmented methylsiloxanes and hydroxylated
26 methylsiloxanes were combined with relevant main cVMS.

27 To minimize interference from other compounds occurring either the same m/z as the main peak or as the
28 isotope peaks, the quantification employed a correction based on the ratios between the isotope peak to
29 the main peak, as elucidated in our prior research (Yao et al., 2022, 2023). While most of the detected
30 ratios between the first isotope peak and the main peak (labeled $(\text{M}+1)/\text{M}$) corresponded to the theoretical
31 value, deviations could still be observed. If the $(\text{M}+1)/\text{M}$ ratio exceeds the theoretical ratio, it is assumed
32 that the main peak has less interference, and that interfering compounds are likely present on the first
33 isotope peak. Conversely, if $(\text{M}+1)/\text{M}$ is less than the theoretical ratio, but still significantly higher than
34 expected for CHON hydrocarbons, interfering compounds might be present at the m/z of the main peak.
35 The total concentration of the methylsiloxanes is calculated based on the peak with less interference. The
36 concentration of the main or isotope peak is divided by the theoretical mass fraction of this specific peak
37 in the total mass (including the main peak and all isotope peaks). Sometimes the ratios between the second
38 isotope peak and the main peak $(\text{M}+2)/\text{M}$ were higher than the theoretical ratios. This is probably due to

39 the fact that hydroxylated methylsiloxanes occur at roughly the same m/z as the second isotope peak. To
40 quantify hydroxylated methylsiloxanes, the mass of the second isotope peak of the corresponding cVMS
41 is estimated based on theoretical $M/(M+2)$ ratios and subtracted from the higher peak at $m/z + 2$. For the
42 purpose of this study, the fragmented methylsiloxanes and hydroxylated methylsiloxanes were combined
43 with the relevant main cVMS in the calculation and presentation of the results.

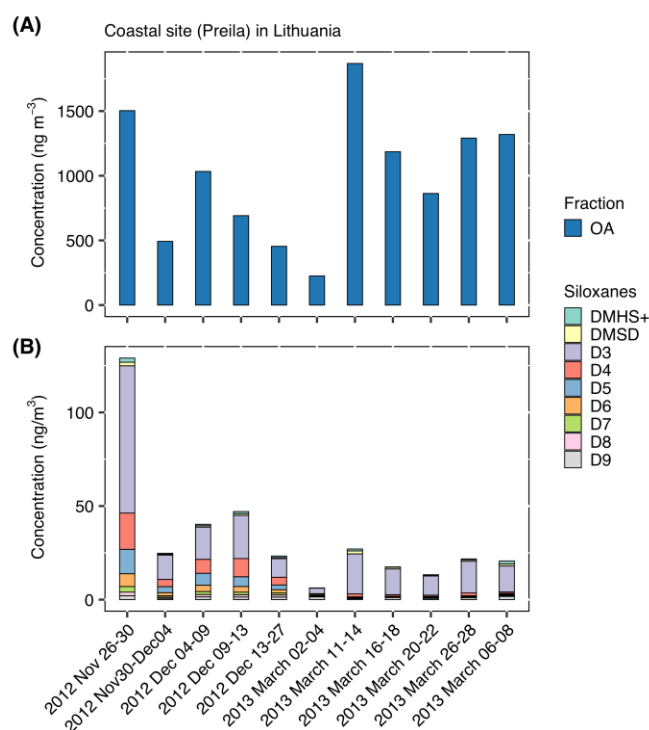
44 The particulate matter sampling and PTR-MS measurements were carried out by different researchers at
45 different periods, resulting in variations in mass resolution and working conditions of the equipment. As
46 a result, the detected methylsiloxanes showed slight differences in subsequent discussion. However, the
47 overall identification of methylsiloxanes and their derivatives remained consistent, and the trends
48 observed in thermal desorption and depolymerization were also similar. In addition, the high m/z (> 400)
49 molecules may experience a slight underestimation according to transmission curves, attributable to the
50 inevitable effects of detector aging in PTR-MS.

51

52 **Note S1. Methylsiloxanes in particulate matter samples collected in Lithuania**

53 Methylsiloxanes and derivatives, including fragments, were identified in particulate matter samples
54 collected from coastal, urban, and forest regions in Lithuania. The concentrations of organic aerosols
55 (OA) and methylsiloxanes (DMHS⁺, DMSD, D₃–D₉) are shown in Figs. S1–S3.

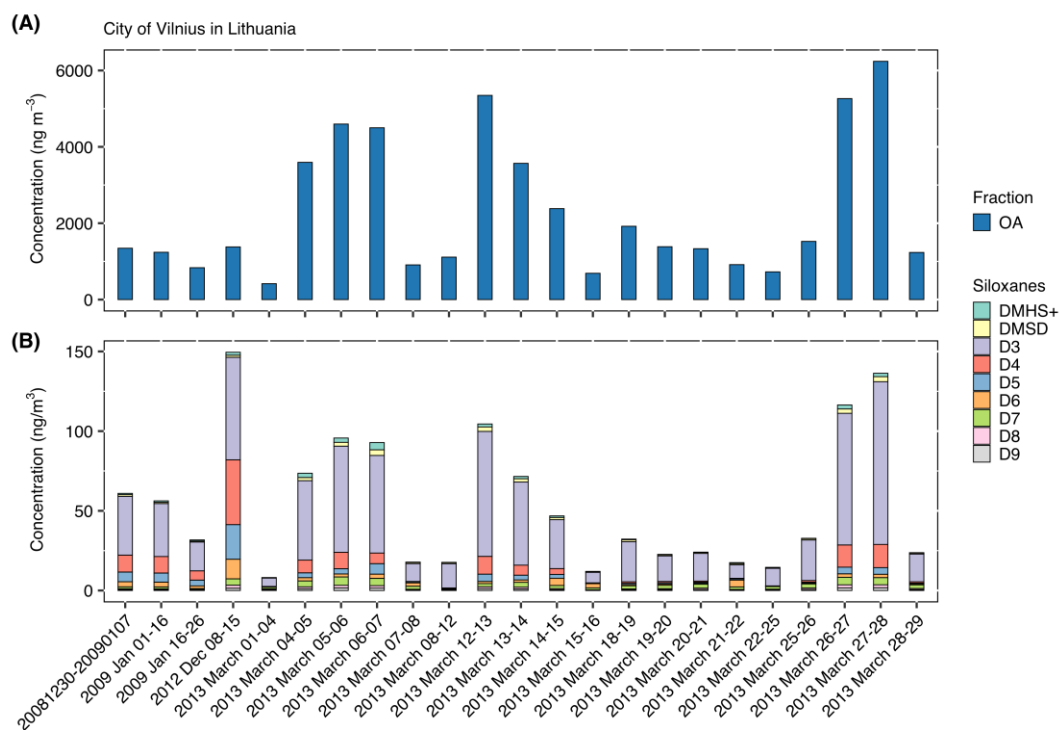
56



57

58 **Fig. S1. Concentrations of (A) organic aerosols and (B) methylsiloxanes in particulate matter**
59 **samples collected from a coastal site (Preila) in Lithuania.**

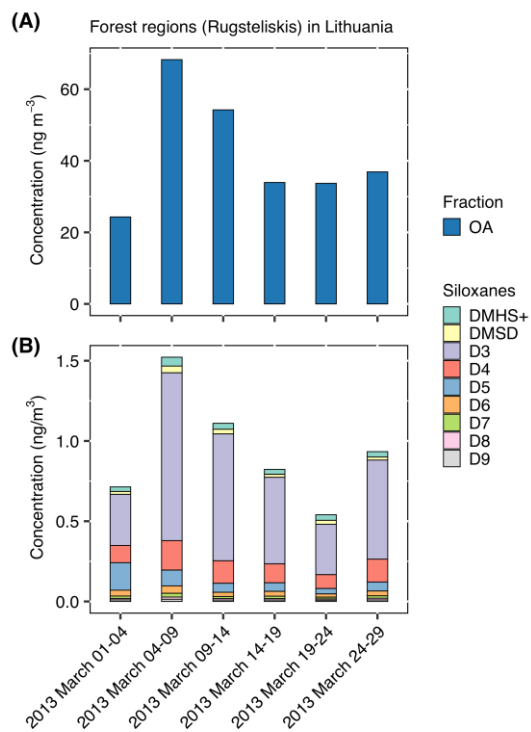
60



61

62 **Fig. S2. Concentrations of (A) organic aerosols and (B) methylsiloxanes in particulate matter**
 63 **samples collected in the city of Vilnius in Lithuania.**

64



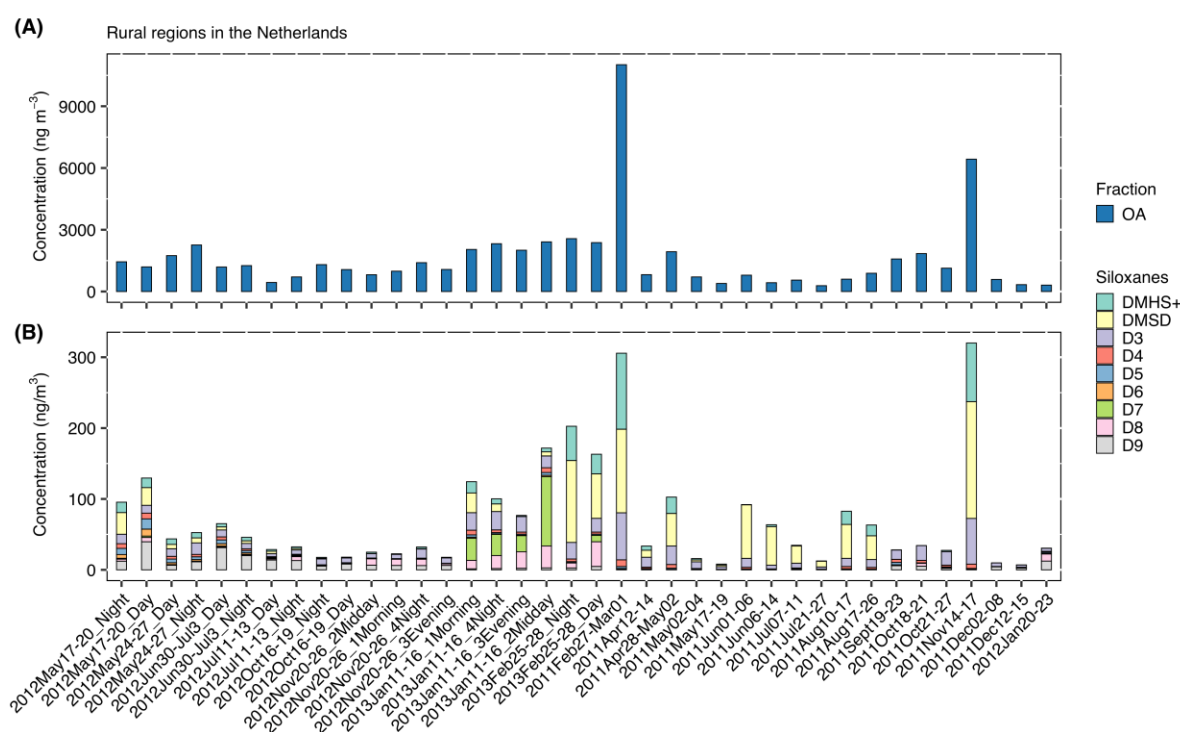
65

66 **Fig. S3. Concentrations of (A) organic aerosols and (B) methylsiloxanes in particulate matter**
 67 **samples collected from forests (Rugsteliskis) in Lithuania.**

68

69 **Note S2. Methylsiloxanes in particulate matter samples collected in the Netherlands**

70 Methylsiloxanes and derivatives, including fragments, were identified in particulate matter samples
 71 collected from rural regions of the Netherlands. The concentrations of OA and methylsiloxanes (DMHS⁺,
 72 DMSD, D₃–D₉) are shown in Fig. S4. Verification of D₃–D₉ was established through the evaluation of
 73 the ratios between isotope peaks and main peaks, thereby confirming their presence. DMHS⁺ and DMSD
 74 were exclusively identified by their m/z ratio, but their presence was confirmed as monomeric fragments
 75 of larger methylsiloxanes during the analysis of methylsiloxane standard samples. They are usually
 76 present in small amounts. However, in certain samples collected in the Netherlands, the levels of DMHS⁺
 77 and DMSD were notably high, indicating the possible presence of other compounds with the same m/z
 78 ratios. Consequently, only the validated D₃–D₉ components were considered for the calculation, whereas
 79 DMHS⁺ and DMSD were disregarded in this specific dataset for the Netherlands, potentially leading to a
 80 slight underestimation.



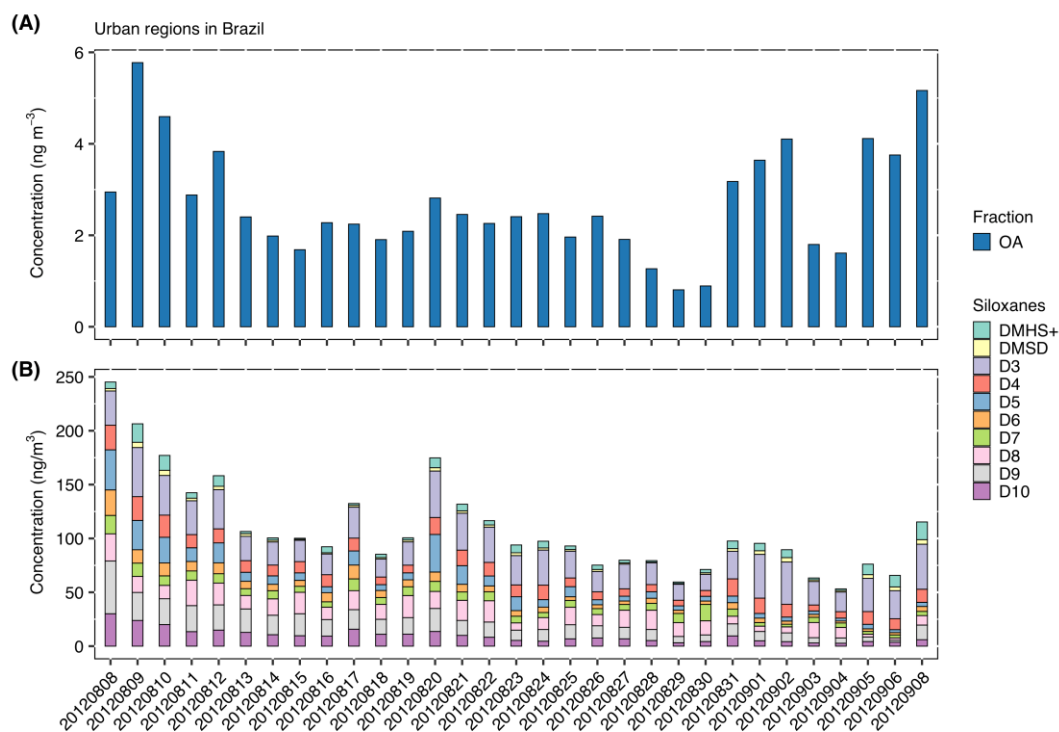
81

82 **Fig. S4. Concentrations of (A) organic aerosols and (B) methylsiloxanes in particulate matter**
 83 **samples collected from rural regions (Cabauw) in the Netherlands.**

84 **Note S3. Methylsiloxanes in particulate matter samples collected in São Paulo, Brazil**

85 Methylsiloxanes and derivatives, including fragments, were identified in particulate matter samples
 86 collected from urban regions in São Paulo, Brazil. The concentrations of OA and methylsiloxanes
 87 (DMHS⁺, DMSD, D₃–D₁₀) are shown in Fig. S5.

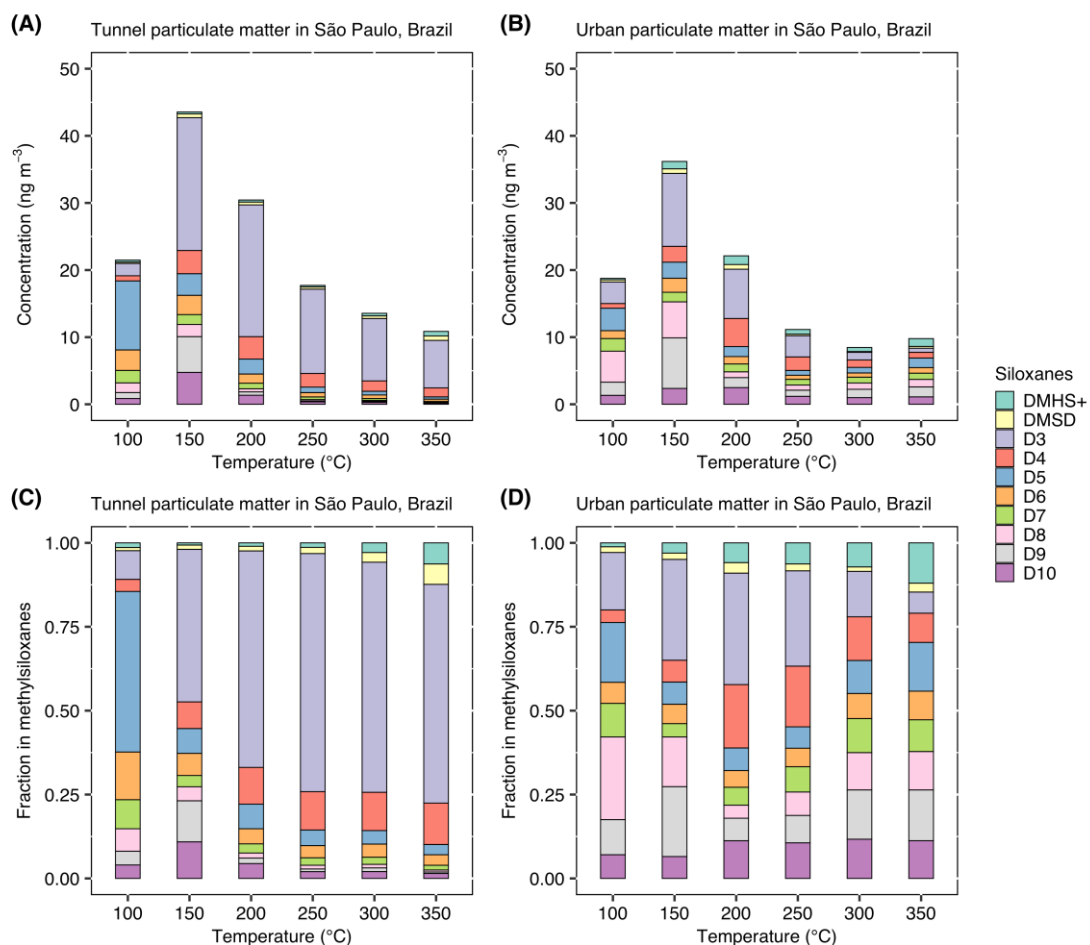
88



89

90 **Fig. S5. Concentrations of (A) organic aerosols and (B) methylsiloxanes in particulate matter**
 91 **samples collected from urban regions in São Paulo, Brazil.**

92



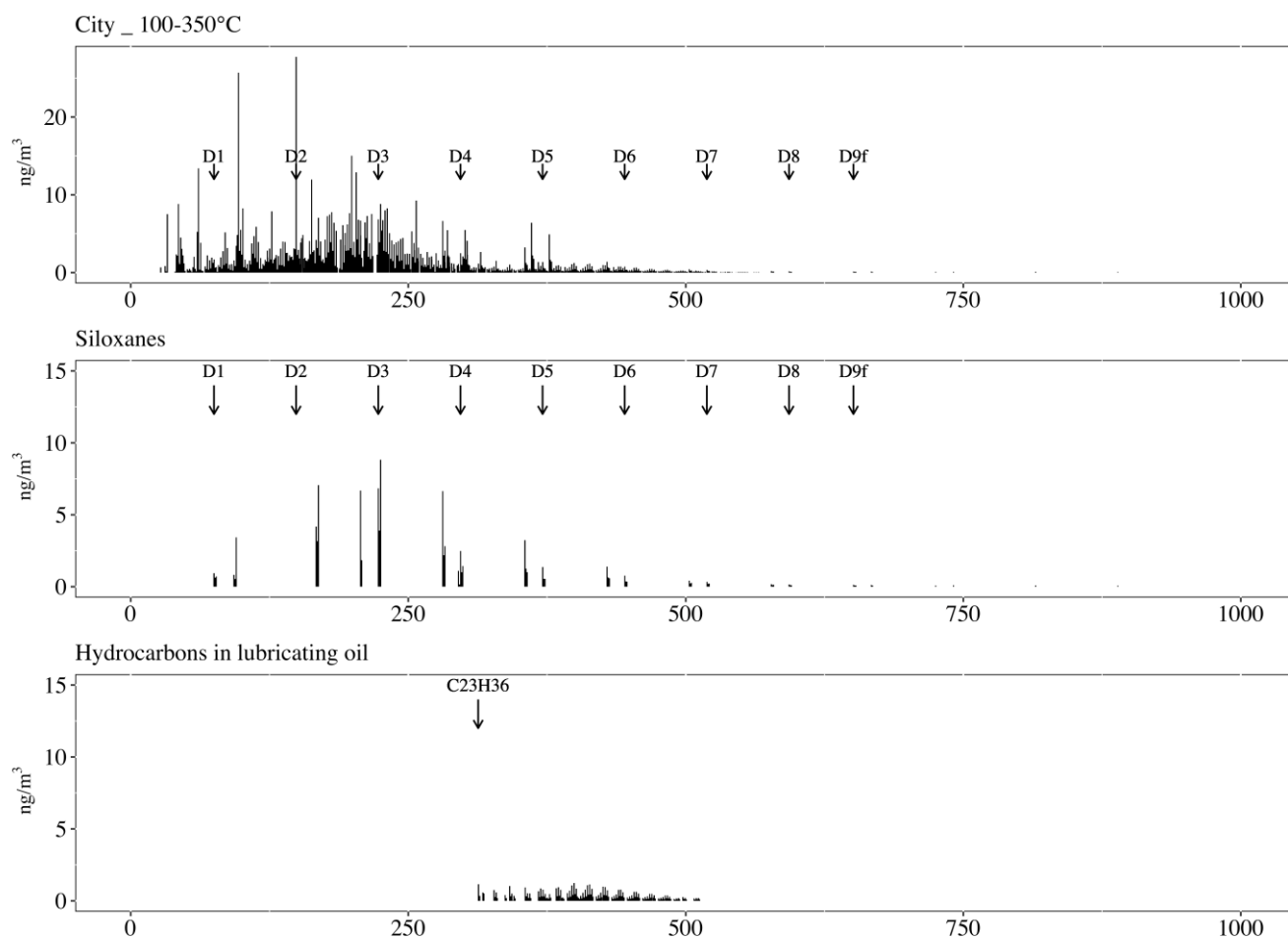
94

95 **Fig. S6. Thermal desorption and depolymerization of methylsiloxanes from particulate matter filter**
 96 **samples in São Paulo, Brazil.** Concentrations of various methylsiloxanes as a function of desorption
 97 temperature in **(A)** tunnel and **(B)** urban particulate matter. Fraction of various detected methylsiloxanes
 98 in the total methylsiloxane content for **(C)** tunnel and **(D)** urban particulate matter.

99

100 Figures S7–S8 present representative mass spectra of aerosols from urban and coastal regions in
101 Lithuania. Methylsiloxane and hydrocarbon peaks are several orders of magnitude higher than those of
102 other compounds, allowing for their identification and quantification with minimal interference from
103 CHONS compounds.

104



105

106 **Fig. S7. Representative mass spectra of aerosols from an urban region in Lithuania.**

107

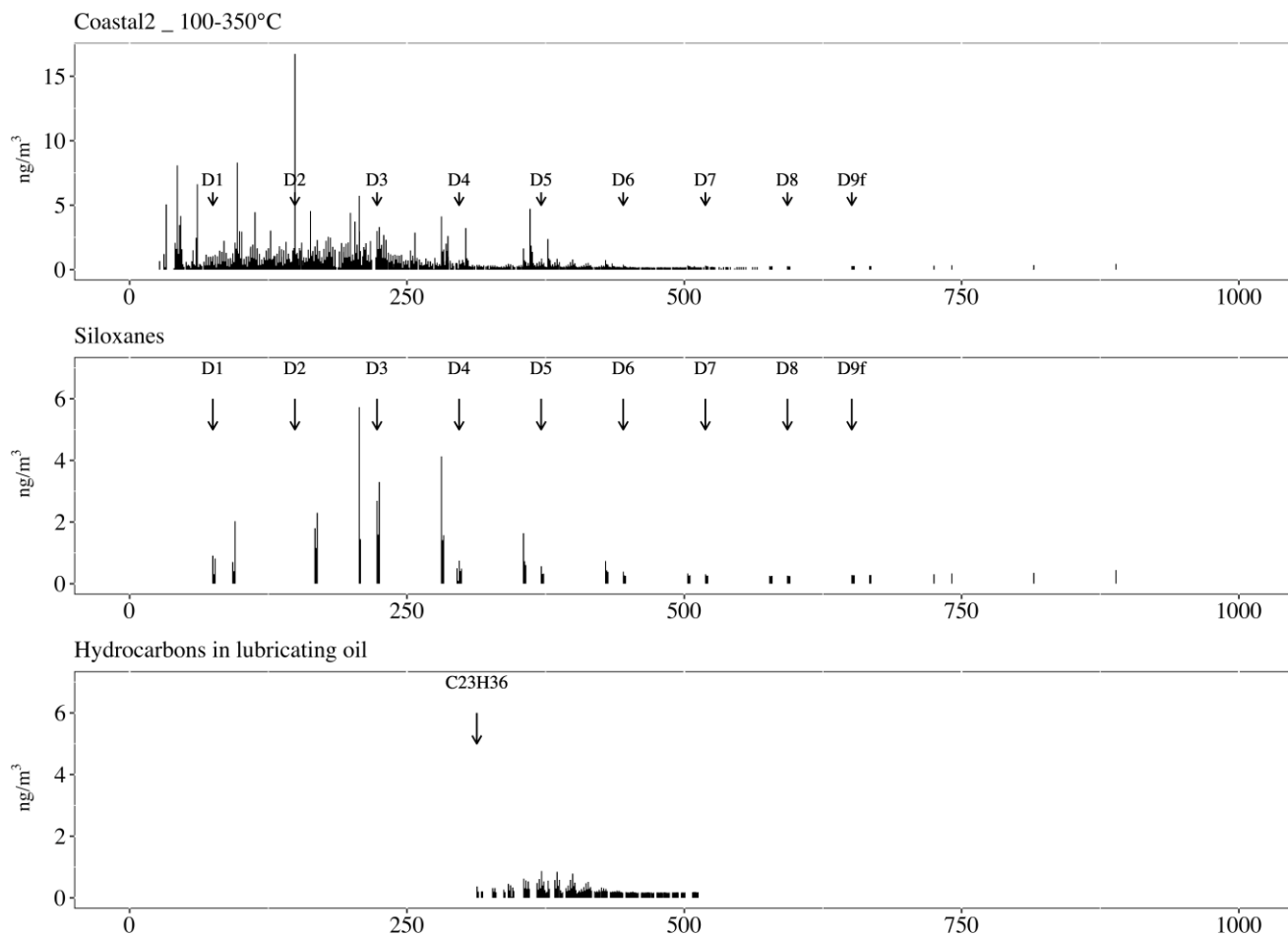
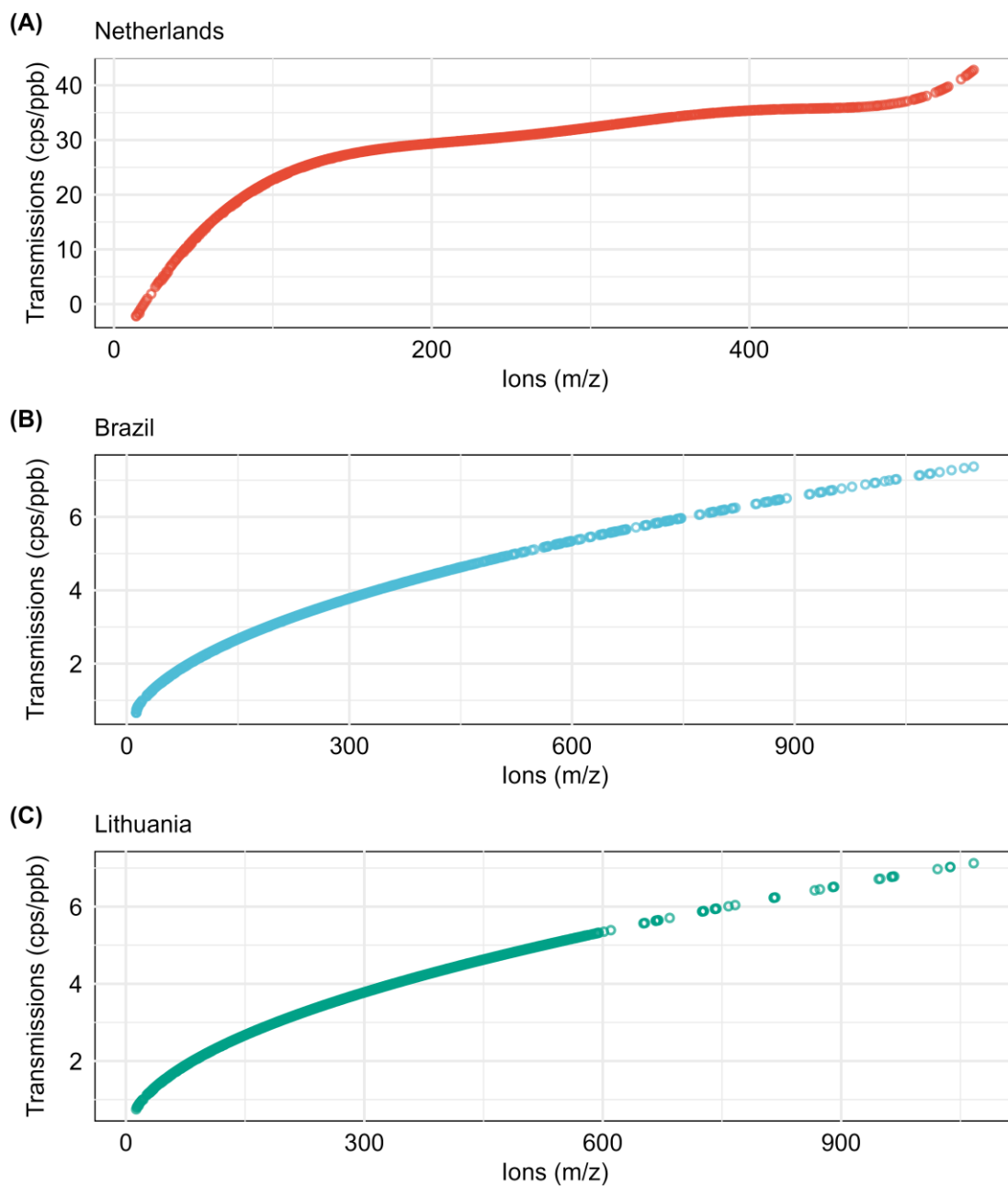


Fig. S8. Representative mass spectra of aerosols from a coastal region in Lithuania.

111 Before analysis, PTR-MS is calibrated using multi-component standard gases to establish a transmission
112 curve (Holzinger, 2015; Worton et al., 2023). These standard gases contain compounds with different
113 molecular weights and known concentrations. The calibration process involves introducing the standard
114 gases into the PTR-MS, measuring the corresponding mass spectral signal intensities, and deriving a
115 transmission curve that quantifies the relationship between concentration and signal intensity. For sample
116 analysis, PTR-MS signal intensities are converted into ppb concentrations in the N₂ carrier gas based on
117 this transmission curve.

118



119

120 **Fig. S9. Transmissions of PTR-MS for the measurements conducted in this study. (A) Netherlands.**

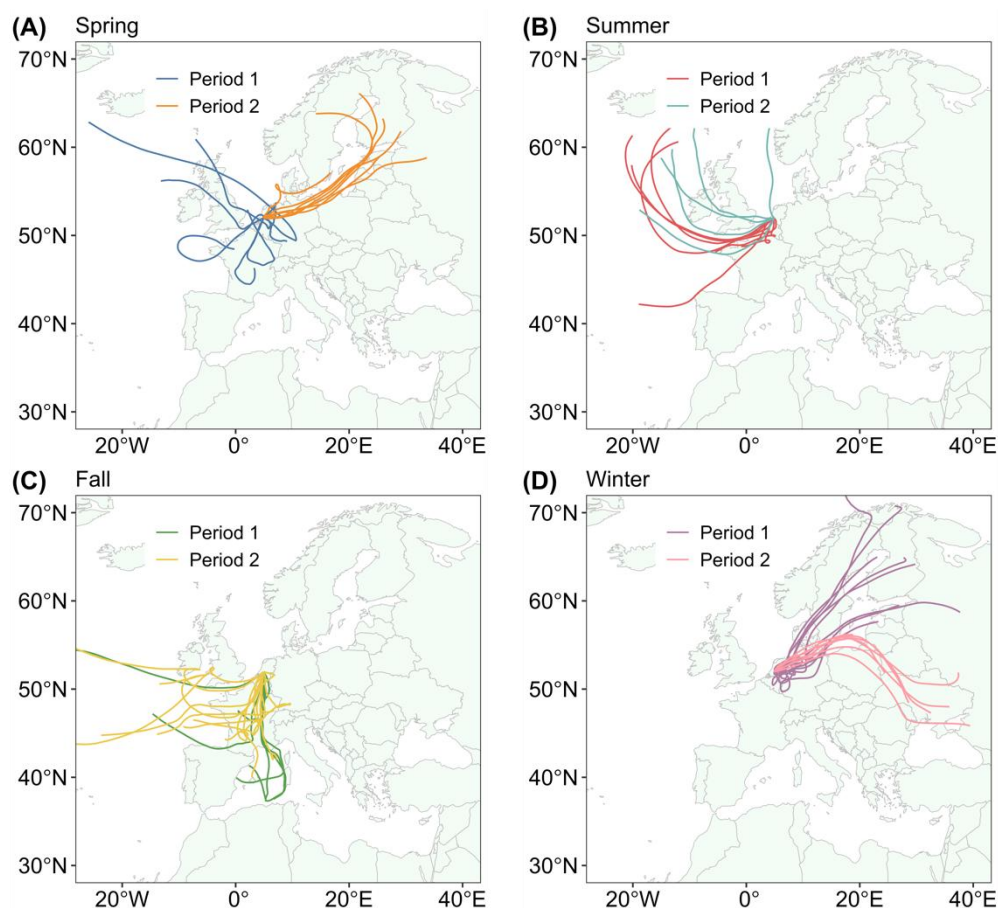
121 (B) Brazil. (C) Lithuania.

122

123 **Note S5. Air mass back trajectories at the Cesar Observatory, Netherlands**

124 Three-day air mass back trajectories were computed using HYSPLIT model (Stein et al., 2015) at a 100
125 m arrival height for the receptor site at the Cesar Observatory, Netherlands, as shown in Fig. S10.
126 Sampling was conducted in two distinct periods within each season throughout 2011–2012.

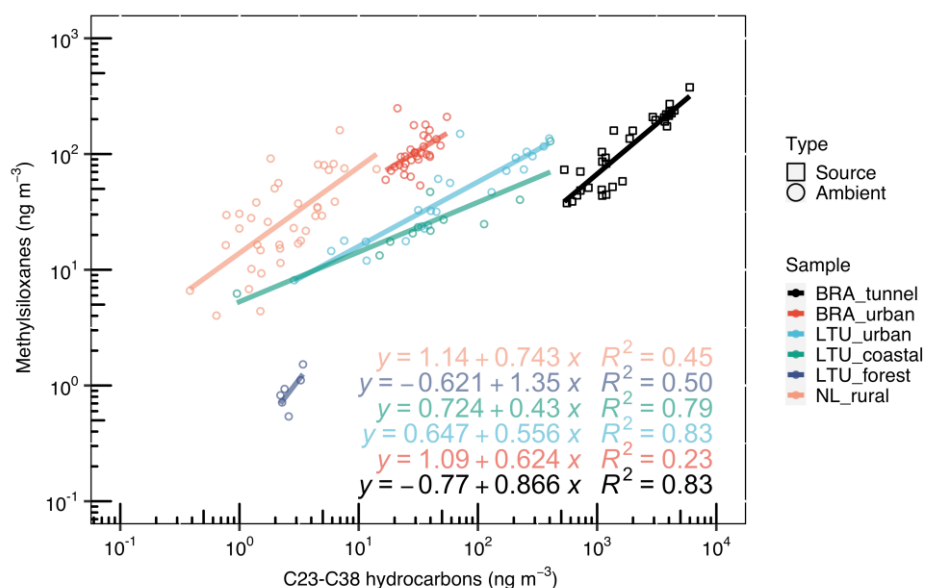
127



128

129 **Fig. S10. Three-day air mass back trajectory computed at a 100 m arrival height for the receptor**
130 **site at the Cesar Observatory, Netherlands during 2011–2012: (A) Spring, (B) Summer, (C) Fall, and**
131 **(D) Winter.**

132



134

135 **Fig. S11. Scatter plot and linear regressions of methylsiloxanes versus C₂₃–C₃₈ hydrocarbons in**
 136 **tunnel and atmospheric particulate matter.** The tunnel particulate matter was collected in São Paulo
 137 (Brazil, BR), while ambient samples include atmospheric particulate matter collected in São Paulo,
 138 Lithuania (LTU), and the Netherlands (NL).

139

140 **Method S2. Inhalation rates of methylsiloxanes, PFAS, and micro-/nanoplastics in atmospheric**
141 **particulate matter**

142 The calculation of the 24-hour inhalation rate can be expressed as follows:

143
$$IR = V \times C \quad (S1)$$

144 where V refers to the daily air inhalation volume for the child or adult, and C refers to the mass
145 concentration of pollutant in the air.

146 Previous research has suggested that 24-hour inhalation volumes for various age groups can be effectively
147 represented by log-normal probability density functions (PDFs) (Allan and Richardson, 1998). These
148 distributions are characterized by arithmetic mean values and standard deviations as follows:
149 approximately $9.3 \pm 2.4 \text{ m}^3 \text{ day}^{-1}$ for toddlers, $14.6 \pm 3.0 \text{ m}^3 \text{ day}^{-1}$ for children, $15.8 \pm 3.7 \text{ m}^3 \text{ day}^{-1}$ for
150 teenagers, $16.2 \pm 3.8 \text{ m}^3 \text{ day}^{-1}$ for adults, and $14.2 \pm 3.3 \text{ m}^3 \text{ day}^{-1}$ for seniors (Allan and Richardson, 1998;
151 Stifelman, 2007). An existing study used a lognormal distribution for adult and normal distribution for
152 child (Mohamed Nor et al., 2021). In this study, we employed log-normal distribution, and the age groups
153 were amalgamated into two categories, i.e., child (toddlers, children, and teenagers) and adult (adults and
154 seniors). Specifically, the distribution of each group was first discretized into 10000 data points, and the
155 two categories were then combined using the Monte Carlo method. The ensuing ranges, subsequently
156 presented, pertain to the 90% confidence interval.

157 Methylsiloxanes present within atmospheric particulate matter can be inhaled along with the particulate
158 components. Consequently, the inhalation rate can be estimated based on the methylsiloxanes
159 concentrations obtained in this study, as shown in Fig. 4a. Notably, the actual inhalation rates should be
160 higher, given that only methylsiloxanes desorbing from filter samples at temperatures below 350 °C were
161 considered herein. In the context of PFAS, their detection through chemical analysis in the literature is
162 typically reported in mass concentration (Evich et al., 2022), which can directly be used in Equation S1.
163 Based on recent statistical insights (Faust, 2023), an estimation of inhalation rates of PFAS through

164 atmospheric particulate matter was attained, as shown in Fig. 4b. In the case of micro- and nanoplastics,
165 first their mass concentrations were estimated as explained in Model S1, and then the inhalation rates
166 were determined using Equation S1.

167

168 **Model S1. Mass concentration of micro- and nanoplastics**

169 Microplastics are typically categorized within the size range of 1 to 5000 μm , whereas plastic particles
170 smaller than 1 μm are commonly denoted as nanoplastics. Since most studies report micro- and
171 nanoplastics in terms of particle numbers per cubic meter (MP m^{-3}), their mass concentrations are not
172 readily available. Previous research estimated the inhalation rates of microplastics in the size range of 1–
173 5000 μm (Mohamed Nor et al., 2021). However, not all microplastic sizes within this range are inhalable,
174 and nanoplastics were frequently disregarded.

175 Recent studies have given more insights into the properties of micro- and nanoplastics by reporting
176 probability density functions of particle size and various other characteristics. These continuous
177 distributions can be incorporated into the Monte Carlo method. Based on these probability density
178 functions, we estimated the human inhalation rates of micro- and nanoplastics with sizes below 10 μm
179 using Monte Carlo simulations, as follows:

$$180 \quad C_{mass} = C_{number} \times \sum_{Morphotype} \left(\sum_{1 \mu m}^{10 \mu m} V(d) \times \rho \right) \times \frac{1}{1 - PM_1/PM_{10}} \quad (S2)$$

181 where C_{mass} refers to distribution of mass concentrations of micro- and nanoplastics, C_{number} refers to
182 distribution of number distribution of microplastics, $Morphotype$ refers to the percentage of microplastics
183 of different shapes, $V(d)$ refers to the particle volume distribution calculated based on the shapes and size
184 distribution (d) between 1–10 μm , ρ refers to density distribution, PM_1/PM_{10} refers to the distribution of
185 mass ratio between PM_1 and PM_{10} of micro- and nanoplastics.

186

187 **Model S1.1 Particle number concentration of microplastics**

188 For microplastics concentrations, we mainly consider studies based on active sampling, primarily due to
189 the rapid settling behavior of larger particles. This tendency could potentially lead to differences between

190 particulate matter suspended in the air (aerosol) and those that settle on the ground (dust). Moreover, large
191 particles cannot be inhaled into the lungs. The inhalation rates would be overestimated if passive sampling
192 results were included. Additionally, existing results from the literature are insufficient to effectively
193 deduce concentration distributions, as some of the concentrations were summarized as ranges.

194 Drawing from recent studies, microplastic levels in both indoor and outdoor air were reported within the
195 range of 0.01 to 5650 MP m⁻³ (Revell et al., 2021; Allen et al., 2022). Notably, concentrations are lower
196 in rural and marine areas, e.g., 0.9 MP m⁻³ in the outdoor air of rural Paris, 0.06–1.37 MP m⁻³ across the
197 North Atlantic Ocean, South China Sea, Indian Ocean, and Western Pacific Ocean. Conversely, higher
198 concentrations were found close to urban areas, e.g., 5650 MP m⁻³ in outdoor air in Beijing (Li et al.,
199 2020). A recent study adopted 100 MP m⁻³ as a global average to calculate direct radiative effects (Revell
200 et al., 2021), and another study employed 36.3 MP m⁻³ as the median concentration (Mohamed Nor et al.,
201 2021). Considering these insights, we selected 36.3 MP m⁻³ and 100 MP m⁻³ as the median and mean
202 concentrations, and we presumed a log-normal distribution of the concentration. Based on this, the
203 parameters of the log-normal distribution can be determined to be 3.592 and 1.423 for arithmetic mean
204 value and standard deviation, and the Monte Carlo method was employed. The minimum and maximum
205 values 0.01 MP m⁻³ and 5650 MP m⁻³ from literature were also shown in Fig. 4c as extreme cases for
206 comparison.

207

208 **Model S1.2 Particle number concentration of nanoplastics**

209 The prevalence of particle number concentrations in microplastics research has established Fourier-
210 transform infrared spectroscopy (FTIR) and Raman spectroscopy as pervasive methodologies. However,
211 widely utilized methods such as FTIR and Raman encounter limitations in accurately measuring
212 nanoplastics due to size constraints. Specifically, micro-Fourier transform infrared (μFTIR) is constrained
213 to sizes down to 11 μm, μRaman to 2 μm, FTIR to 10 μm, and Raman to 1 μm (Revell et al., 2021; Allen

214 et al., 2022; Xu et al., 2019; Zheng et al., 2021; Caputo et al., 2021; Mitrano et al., 2021; Cai et al., 2021;
215 Velimirovic et al., 2021a). These limitations make the detection of nanoplastics challenging, leading to a
216 limited understanding of their number concentrations.

217 Pyrolysis-based mass spectrometry methods have gained prominence in response to increasing interest in
218 the field (Picó and Barceló, 2020; Ivleva, 2021; Velimirovic et al., 2021b). However, their potential is
219 offset by challenges such as complexity and time-intensive procedures compared to the more prevalent
220 and expedient FTIR and Raman techniques. Furthermore, the prevalent reporting of number
221 concentrations over mass concentrations by microplastics researchers has constrained the adoption of
222 pyrolysis-based methods. Consequently, the availability of these methodologies has not resulted in a
223 commensurate increase in related scientific publications.

224 Aerosol researchers possess a strategic advantage in nanoplastics analysis compared to those in water and
225 soil studies. Recent breakthroughs, facilitated by size separation methods in aerosol science, have resulted
226 in significant advancements, enabling the quantification of nanoplastics using pyrolysis-based mass
227 spectrometry methods (Kirchsteiger et al., 2023; Sheng et al., 2023). However, these two studies reveal
228 divergent concentration ranges, with one in the ng m^{-3} range and the other in the pg m^{-3} range.

229 Several previous studies have already employed pyrolysis-based mass spectrometry methods to assess
230 microplastics in total particulate matter (PM, without size separation), PM_{10} , and $\text{PM}_{2.5}$ (Peñalver et al.,
231 2021; Goßmann et al., 2023; Costa-Gómez et al., 2023; Mizuguchi et al., 2023; Fan et al., 2022; Luo et
232 al., 2023). Given the particle size cutting has only an upper limit, the measured microplastics actually
233 encompass nanoplastics. However, the number of existing studies is very limited, and these studies
234 reported mass concentrations of airborne microplastics (and nanoplastics) across six to seven orders of
235 magnitude, also from pg m^{-3} to $\text{sub-}\mu\text{g m}^{-3}$, suggesting potential overestimation and underestimation
236 contingent on methods and strategies employed by distinct research groups. Divergences could arise from
237 differences in mass peak recognition and correction methods, necessitating further research for fair

238 comparison and evaluation. Due to the very limited existing studies and the insufficient maturity of the
239 pyrolysis-based mass spectrometry methods, it is too early to summarize global average mass
240 concentrations of microplastics or nanoplastics based on the results from pyrolysis-based methods. As a
241 result, we still estimate the mass concentrations of microplastics and nanoplastics based on the modeling
242 method, and the estimation of mass concentrations of nanoplastics described in Model S1.7.

243

244 **Model S1.3 Morphotype**

245 Micro- and nanoplastics were found to encompass various morphotypes, including fibers, beads, and
246 films. Recent investigations report the median frequencies of fibers, fragments, and films as
247 approximately 60%, 35%, and 20%, respectively (not normalized to unity; normalized to 52.2%, 30.4%,
248 and 17.4%) (Revell et al., 2021). Since films are relatively less prevalent than other morphotypes, and
249 information regarding their size distribution remains limited, they were omitted from subsequent analyses
250 (Kooi and Koelmans, 2019). To bridge this gap, we presume the median frequencies to be a composite of
251 50% fragments and 50% fibers (Revell et al., 2021).

252

253 **Model S1.4 Aspect ratio**

254 To simplify the calculations, all fragments of micro- and nanoplastics were treated as spheres during
255 computations. Meanwhile, fibers were considered as cylinders. According to a previous study, the length
256 (L) and diameter (D) of the fiber are related according to the following equation (Revell et al., 2021):

$$257 \quad D = A \log \left(1 + \frac{L}{B} \right) \quad (S3)$$

258 where A = 6 μm and B = 30 μm (Revell et al., 2021).

259

260 **Model S1.5 Size distribution**

261 In previous studies, the size distributions of microplastics were found to align well with the gamma
262 distribution (Revell et al., 2021). For fragments, a gamma distribution with the shape parameter of 2 and
263 the scale parameter of 15 μm was assumed. For fiber lengths, a gamma distribution was applied with a
264 shape parameter of 2.5 and a scale parameter of 250 μm . Some studies have also advocated for a log-
265 normal size distribution (Kooi and Koelmans, 2019; Koelmans et al., 2020). Another has proposed that
266 the size distribution of the microplastic particle size often follows to a power law with a negative exponent
267 (Koelmans et al., 2022). This specific study suggested a size median of 20 μm within the range of 1–5000.
268 Although the debates persist, we opted to employ the gamma distribution for our analysis.

269 Microplastics encompass a range of particle sizes from 1 to 5000 μm ; however, only particles smaller
270 than 10 μm (PM_{10}) can be inhaled, and those below 2.5 μm ($\text{PM}_{2.5}$) have a higher probability to enter the
271 lungs. In this study, inhalable micro- and nanoplastics were considered to be smaller than 10 μm .

272

273 **Model S1.6 Density distribution**

274 Microplastic polymers exhibit a density range spanning approximately 0.8–2 g cm^{-3} , with the most
275 prevalent density around 1 g cm^{-3} . An environmentally relevant microplastic particle on average has a
276 weight of 12.5 μg , a volume of 0.011 mm^3 and a density of 1.14 g cm^{-3} (Koelmans et al., 2022). According
277 to another study, the density ranges from 0.86 g cm^{-3} for polyethylene to 1.38 g cm^{-3} for polyethylene
278 terephthalate and polyvinyl chloride (Revell et al., 2021). Furthermore, an alternate study indicated the
279 density distribution of microplastics conforming to the normal-inverse Gaussian shape, characterized by
280 $\alpha = 75.1$, $\beta = 71.3$, $\delta = 0.097$, and $\mu = 0.84$ (Kooi and Koelmans, 2019). In this study, the normal-inverse
281 Gaussian shape was adopted for computational purposes.

282

283 **Model S1.7 Estimation of nanoplastic mass concentration**

284 Earlier investigations documented $PM_{2.5}/PM_{10}$ ratios ranging from 0.44 to 0.85 in different regions of the
285 world (Querol et al., 2008), 0.6 (Eeftens et al., 2012) and 0.44–0.90 (Putaud et al., 2010) in Europe, and
286 0.65 in China (Zhou et al., 2016), highlighting a certain variability in this ratio. Likewise, PM_1/PM_{10} ratios
287 have been reported to range from 0.15 to 0.47 in diverse regions of the world (Querol et al., 2008).

288 Currently, there is no clear evidence that nanoplastics have either higher or lower concentrations than
289 microplastics. Consequently, we posit that nanoplastics are ubiquitous constituents in atmospheric
290 aerosols, with a similar PM_1/PM_{10} ratio as ambient particulate matter. The coefficient for converting
291 microplastic mass concentrations into the total (including micro- and nanoplastic) mass concentrations
292 can be computed as follows:

293
$$\eta = \left(1 + \frac{PM_1}{PM_{10} - PM_1}\right) = \frac{1}{1 - PM_1/PM_{10}} \quad (S4)$$

294 where the PM_1/PM_{10} ratios were presumed to conform to a triangular probability distribution
295 characterized by values $a = 0.15$ (lower limit), $b = 0.31$ (maximum), and $c = 0.47$ (upper limit).

296

297 **Model S1.8 Inhalation volume**

298 Micro- and nanoplastics themselves are forms of particulate matter, distinguishing them from
299 methylsiloxanes and PFAS, which represent potential chemical constituents that might exist within
300 atmospheric particulate matter. The inhalation volume estimated from Method S2 is applicable to micro-
301 and nanoplastics. Employing the Monte Carlo method, we proceed to calculate inhalation rates by
302 synthesizing the distribution of inhalation volumes, incorporating the mass concentration distribution of
303 micro- and nanoplastics, as well as the maximum and minimum concentrations for comparison.

304

305 **Model S1.9 Differences from other models**

306 We have drawn certain assumptions from several preceding modeling studies. One of these studies
307 investigated the role of micro- and nanoplastics as cloud condensation nuclei (CCN) or ice-nucleating
308 particles (INPs), influencing cloud formation (Aeschlimann et al., 2022). Another study assessed direct
309 radiative impacts of airborne microplastics, predominantly focusing on larger microplastic particles while
310 somewhat overlooking smaller counterparts (Revell et al., 2021). These studies, while providing valuable
311 insights, differ slightly from our hypotheses due to divergent focal points. Our research places a distinct
312 emphasis on smaller-sized particles, with a focus on deriving mass concentrations from particle counts.

313

314 **Model S2. Aerosol surface tension and large molecular methylsiloxanes**

315 Large molecular methylsiloxanes possess very low surface tension, and their presence in atmospheric
316 aerosols may influence aerosol surface properties. To illustrate this, we designed a conceptual experiment:
317 assuming the aerosol as a spherical particle, the hydrophobic large molecular methylsiloxanes are
318 expected to reside in the oil phase, thereby altering the oil–water interfacial balance. On this basis, we
319 consider how large molecular methylsiloxanes could affect aerosol surface tension, their ability to act as
320 cloud condensation nuclei (CCN), and the potential magnitude of such impacts.

321 **Model S2.1 Existing observations on aerosol surface tension and CCN activation**

322 The presence of organic coatings on atmospheric droplets contributes to a reduction in surface tension,
323 leading to increased CCN activation (Cruz and Pandis, 1998; Ruehl et al., 2012, 2016) and amplifying
324 cloud albedo effects (Facchini et al., 1999). Early studies measured surface tension, reporting values such
325 as 60.9–72.3 mN m⁻¹ for fog in Dübendorf, Switzerland (Capel et al., 1990), 67.2 mN m⁻¹ for wet aerosol
326 and cloud/fog droplets in the Po Valley, Northern Italy (Facchini et al., 2000), an average of 69.3 mN m⁻¹
327 and a minimum of 60.6 mN m⁻¹ for cloud water collected at the Rax mountain in central Europe
328 (Hitzenberger et al., 2002), 64.4–71.3 mN m⁻¹ for cloud water in Jeju Island, South Korea (Decesari et
329 al., 2005), and 52 mN m⁻¹ for particulate matter in the Amazon basin (Mircea et al., 2005). However,
330 these early studies focused solely on the surface tension of the aqueous phase (cloud water, fog) or the
331 water-extracted fraction of particulate matter, neglecting water-insoluble (hydrophobic) organic matter
332 and underestimating the surface tension of ambient particulate matter (Baduel et al., 2012; Lee and
333 Tivanski, 2021). Incorporating water-insoluble organic matter, the surface tension of ambient particulate
334 matter was found to be 30 mN m⁻¹ in summer and 35–45 mN m⁻¹ in winter in Grenoble, France (Baduel
335 et al., 2012), 32–40 mN m⁻¹ on the Baltic Coast at Askö, Sweden (Gérard et al., 2016), and 49 mN m⁻¹
336 for North Atlantic marine air masses in Ireland (Ovadnevaite et al., 2017). Similarly, water-insoluble

337 methylsiloxanes and long-chain hydrocarbons can impact the surface tension of atmospheric particulate
338 matter.

339

340 **Model S2.2 Density of methylsiloxanes and hydrocarbons**

341 The density of water is around 1 g cm^{-3} at room temperature. Meanwhile, the density of PDMS is around
342 0.97 g cm^{-3} at room temperature and decreases with decreasing the molecular weight, e.g., 0.950 g cm^{-3}
343 for D₄, 0.954 g cm^{-3} for D₅, 0.963 g cm^{-3} for D₆ at 25 °C. Notably, PDMS exhibit significant
344 hydrophobicity, which means that PDMS will separate and float on the water when combined with water.
345 Similarly, hydrocarbons are also hydrophobic, and the densities of hydrocarbons are also lower than water
346 at room temperature and increase with increasing molecular weight, e.g., 0.626 g cm^{-3} for C₅H₁₂, 0.730 g
347 cm^{-3} for C₁₀H₂₂, 0.825 g cm^{-3} for C₂₀H₄₂, 0.883 g cm^{-3} for C₃₀H₆₂, and 0.914 g cm^{-3} for C₄₀H₈₂.

348

349 **Model S2.3 Oil film formation**

350 The evolution of an oil drop on the water surface can be described by the spreading coefficient equation
351 as follows (Harkins, 1952; Winoto et al., 2014; Soloviev et al., 2016):

352
$$S = \sigma_{w/a} - \sigma_{o/a} - \sigma_{o/w} \quad (S5)$$

353 where S denotes the spreading coefficient, and $\sigma_{w/a}$, $\sigma_{o/a}$, and $\sigma_{o/w}$ represent the surface tension of water,
354 the surface tension of oil, and the interfacial tension between oil and water, respectively. When $S \geq 0$,
355 the oil droplet has no equilibrium state and can completely spread, or “wet,” the air-water interface.

356 The surface tension of water ($\sigma_{w/a}$) is 72 mN m^{-1} . The surface tension of PDMS ($\sigma_{o/a}$) was reported in
357 previous studies, e.g., on average 18.9 mN m^{-1} (Gaines, 1969), $15.7\text{--}20 \text{ mN m}^{-1}$ (Kanellopoulos and
358 Owen, 1971), Siloxane surface tension $20.5\text{--}23.5 \text{ mN m}^{-1}$ (Ananthapadmanabhan et al., 1990), $19\text{--}21$
359 mN m^{-1} (Vudayagiri et al., 2013), and $19.9 \pm 0.5 \text{ mN m}^{-1}$ (Chen et al., 2019). The interfacial tension

360 between PDMS and water ($\sigma_{o/w}$) without surfactants was reported in previous studies, e.g., 41.8–44.0 mN
361 m^{-1} (Kanellopoulos and Owen, 1971), 37.8–50 mN m^{-1} (El - Hamouz, 2007), and ~ 32 mN m^{-1} (Nowak
362 et al., 2016). According to the aforementioned data, the spreading coefficient (S) for PDMS and water is
363 above 0, indicating that PDMS will spread across the droplet surface if present.

364 Furthermore, additional surfactants can influence the interfacial tension between PDMS and water
365 (Ghorbanizadeh and Rostami, 2017), and surfactants are very common in atmospheric aerosols. Literature
366 reports have detailed the interfacial tension between PDMS and water ($\sigma_{o/w}$) in the presence of various
367 surfactants, e.g., 10 mN m^{-1} for sodium dodecyl sulphate (SDS) (Kanellopoulos and Owen, 1971), 7.2–
368 9.9 mN m^{-1} for SDS and NaCl (Kanellopoulos and Owen, 1971), 14.7–38.9 mN m^{-1} for SDS and Fatty
369 alcohols or silanols (Kanellopoulos and Owen, 1971), ~ 25 mN m^{-1} for Nigrosine solution (Nowak et al.,
370 2016), and ~ 9 mN m^{-1} for sodium lauryl ether sulphate solution (Nowak et al., 2016). The presence of
371 surfactants further amplifies the spreading coefficient (S) between PDMS and water, underscoring that
372 methylsiloxanes within particulate matter are inclined to envelop the droplet surface.

373 Similarly, long-chain hydrocarbons from lubricants also have the potential to influence the surface tension
374 of traffic-emitted particulate matter. The surface tension of hydrocarbons ($\sigma_{o/a}$) demonstrates a reduction
375 with an increase in molecular weight, e.g., 15.9–27.2 mN m^{-1} for C_5 – C_{16} increased with carbon at 22 °C
376 (Goebel and Lunkenheimer, 1997), and 25.2–28.8 mN m^{-1} for crude oil (Winoto et al., 2014). The
377 interfacial tension between hydrocarbons and water ($\sigma_{o/w}$) without surfactants was also reported in
378 previous studies, e.g., 50–55 mN m^{-1} for n-hydrocarbons and water (Kanellopoulos and Owen, 1971),
379 50–53 mN m^{-1} for C_6 – C_{12} alkane and water at 25 °C (Zeppieri et al., 2001), 50.9–55.2 mN m^{-1} for C_5 –
380 C_{16} hydrocarbons and water (Goebel and Lunkenheimer, 1997), and 18.4–27.4 mN m^{-1} for crude oil and
381 water (Winoto et al., 2014). Furthermore, the interfacial tensions between hydrocarbons and water ($\sigma_{o/w}$)
382 with different surfactants were reported in literature, e.g., 19.3–22.3 mN m^{-1} for petroleum and water with
383 silicone polyether additives (Fraga et al., 2012), 11–20 mN m^{-1} to nearly 0 for crude oil and water with

384 dispersants (Brandvik et al., 2019). The spreading coefficient (S) of hydrocarbons and water is usually
 385 greater than 0, which means that hydrocarbons can expand on the water surface.

386 As evidenced by previous studies, organic compounds are more likely to be present in the surface layer
 387 rather than in the bulk of the droplet (Ruehl et al., 2016), suggesting that methylsiloxanes and long-chain
 388 hydrocarbons could potentially coexist with other water-insoluble organics in the surface layer, as
 389 illustrated in Fig. 4D. Assuming particulate matter as spherical, the ratio between two times the thickness
 390 and the sphere's diameter ranges from 0.003 to 0.007. This ratio decreases during the water absorption
 391 process facilitated by CCN. A key question arises about the complete envelopment of particulate matter
 392 or droplets by methylsiloxanes and long-chain hydrocarbons. As discussed earlier, the surface layer
 393 contains other organic matter suspended on the water, a significant fraction of organic aerosol mass,
 394 including methylsiloxanes and long-chain hydrocarbons. The overall surface tension of particulate matter
 395 or droplets depends on the combined surface tension of methylsiloxanes, long-chain hydrocarbons, and
 396 other organic matter suspended on the water. Both methylsiloxanes and long-chain hydrocarbons possess
 397 characteristics to participate the coverage, including lower density than water, hydrophobic traits, low-
 398 than-zero spreading coefficient, and remarkably low surface tension. Without considering other light
 399 hydrophobic organic matter, methylsiloxanes together with long-chain hydrocarbons will be enough for
 400 an extensive surface layer to envelop particulate matter or droplets.

401

402 **Model S2.4 Large molecular methylsiloxanes altering aerosol surface tension and CCN**

403 The ability of aerosol particle to act as a CCN is given by its critical supersaturation. The critical
 404 supersaturation for cloud droplet activation can be estimated by finding the maximum of the Köhler
 405 equation (Equation S6) (Petters and Kreidenweis, 2007):

$$406 \quad Sc(D) = \frac{D^3 - D_d^3}{D^3 - D_d^3(1 - \kappa)} e^{\frac{4\sigma_s/aM_w}{RT\rho_w D}} \quad (S6)$$

407 where $Sc(D)$ is the water vapor saturation ratio above the surface of an aqueous solution droplet, D is the
408 diameter of the droplet (nm), D_d is the dry particle diameter (nm), κ is the hygroscopicity parameter (-),
409 $\sigma_{s/a}$ is the surface tension of the solution/air interface, M_w is the molecular weight of water (18 g mol⁻¹),
410 R is the universal gas constant (8.314 J K⁻¹ mol⁻¹), T is temperature (e.g., 298.15 K), ρ_w is the density of
411 water (1 g cm⁻³). Particles with a lower Sc are more likely to become cloud droplets.

412 Methylsiloxanes and long-chain hydrocarbons derived from lubricants may significantly lower the surface
413 tension of aerosols (or droplets). This reduction in surface tension lowers the Sc required for cloud droplet
414 activation (Equation S6), thereby increasing the likelihood that these particles will act as cloud
415 condensation nuclei (CCN). If all other factors remain unchanged, and the surface tension of aerosols
416 decreases from 72 mN m⁻¹ to 20 mN m⁻¹ due to the presence of large molecular methylsiloxanes, the
417 $Sc(D)$ value would decrease by as much as $e^{72/20} \approx 37$ times, i.e., by more than an order of magnitude.
418 This would significantly enhance the likelihood of aerosols acting as cloud condensation nuclei. As a
419 result, even hydrophobic particles may contribute to cloud formation. Given the widespread occurrence
420 of methylsiloxanes and long-chain hydrocarbons in atmospheric particulate matter, their potential to
421 enhance CCN concentrations could suppress precipitation and increase cloud albedo (Rosenfeld et al.,
422 2014), representing a potentially important but underrecognized influence on climate. However, the
423 magnitude of this impact remains unknown. Experimental confirmation of their enhancement of CCN
424 activity and, if applicable, quantification of their regional and global effects on cloud microphysics and
425 precipitation patterns requires further investigation. Additionally, atmospheric processing of
426 methylsiloxanes may further alter the aerosol, warranting further study.

427

428 **References**

- 429 Aeschlimann, M., Li, G., Kanji, Z. A., and Mitrano, D. M.: Potential impacts of atmospheric microplastics
430 and nanoplastics on cloud formation processes, *Nat. Geosci.*, 15, 967–975,
431 <https://doi.org/10.1038/s41561-022-01051-9>, 2022.
- 432 Allan, M. and Richardson, G. M.: Probability Density Functions Describing 24-Hour Inhalation Rates For
433 Use in Human Health Risk Assessments, *Hum. Ecol. Risk Assess. An Int. J.*, 4, 379–408,
434 <https://doi.org/10.1080/10807039891284389>, 1998.
- 435 Allen, D., Allen, S., Abbasi, S., Baker, A., Bergmann, M., Brahney, J., Butler, T., Duce, R. A., Eckhardt,
436 S., Evangeliou, N., Jickells, T., Kanakidou, M., Kershaw, P., Laj, P., Levermore, J., Li, D., Liss, P., Liu,
437 K., Mahowald, N., Masque, P., Materić, D., Mayes, A. G., McGinnity, P., Osvath, I., Prather, K. A.,
438 Prospero, J. M., Revell, L. E., Sander, S. G., Shim, W. J., Slade, J., Stein, A., Tarasova, O., and Wright,
439 S.: Microplastics and nanoplastics in the marine-atmosphere environment, *Nat. Rev. Earth Environ.*, 3,
440 393–405, <https://doi.org/10.1038/s43017-022-00292-x>, 2022.
- 441 Ananthapadmanabhan, K. P., Goddard, E. D., and Chandar, P.: A study of the solution, interfacial and
442 wetting properties of silicone surfactants, *Colloids and Surfaces*, 44, 281–297,
443 [https://doi.org/10.1016/0166-6622\(90\)80202-F](https://doi.org/10.1016/0166-6622(90)80202-F), 1990.
- 444 Baduel, C., Nozière, B., and Jaffrezo, J.: Summer/winter variability of the surfactants in aerosols from
445 Grenoble, France, *Atmos. Environ.*, 47, 413–420, <https://doi.org/10.1016/j.atmosenv.2011.10.040>, 2012.
- 446 Brandvik, P. J., Daling, P. S., Leirvik, F., and Krause, D. F.: Interfacial tension between oil and seawater
447 as a function of dispersant dosage, *Mar. Pollut. Bull.*, 143, 109–114,
448 <https://doi.org/10.1016/j.marpolbul.2019.04.019>, 2019.
- 449 Cai, H., Xu, E. G., Du, F., Li, R., Liu, J., and Shi, H.: Analysis of environmental nanoplastics: Progress
450 and challenges, *Chem. Eng. J.*, 410, 128208, <https://doi.org/10.1016/j.cej.2020.128208>, 2021.

451 Capel, P. D., Gunde, R., Zuercher, F., and Giger, W.: Carbon speciation and surface tension of fog,
 452 Environ. Sci. Technol., 24, 722–727, <https://doi.org/10.1021/es00075a017>, 1990.

453 Caputo, F., Vogel, R., Savage, J., Vella, G., Law, A., Della Camera, G., Hannon, G., Peacock, B., Mehn,
 454 D., Ponti, J., Geiss, O., Aubert, D., Prina-Mello, A., and Calzolari, L.: Measuring particle size distribution
 455 and mass concentration of nanoplastics and microplastics: addressing some analytical challenges in the
 456 sub-micron size range, J. Colloid Interface Sci., 588, 401–417, <https://doi.org/10.1016/j.jcis.2020.12.039>,
 457 2021.

458 Chen, J., Huang, X., He, L., and Luo, X.: Foaming of Oils: Effect of Poly(dimethylsiloxanes) and Silica
 459 Nanoparticles, ACS Omega, 4, 6502–6510, <https://doi.org/10.1021/acsomega.9b00347>, 2019.

460 Costa-Gómez, I., Suarez-Suarez, M., Moreno, J. M., Moreno-Grau, S., Negral, L., Arroyo-Manzanares,
 461 N., López-García, I., and Peñalver, R.: A novel application of thermogravimetry-mass spectrometry for
 462 polystyrene quantification in the PM₁₀ and PM_{2.5} fractions of airborne microplastics, Sci. Total Environ.,
 463 856, 159041, <https://doi.org/10.1016/j.scitotenv.2022.159041>, 2023.

464 Cruz, C. N. and Pandis, S. N.: The effect of organic coatings on the cloud condensation nuclei activation
 465 of inorganic atmospheric aerosol, J. Geophys. Res. Atmos., 103, 13111–13123,
 466 <https://doi.org/10.1029/98JD00979>, 1998.

467 Decesari, S., Facchini, M. C., Fuzzi, S., McFiggans, G. B., Coe, H., and Bower, K. N.: The water-soluble
 468 organic component of size-segregated aerosol, cloud water and wet depositions from Jeju Island during
 469 ACE-Asia, Atmos. Environ., 39, 211–222, <https://doi.org/10.1016/j.atmosenv.2004.09.049>, 2005.

470 Eeftens, M., Tsai, M.-Y., Ampe, C., Anwander, B., Beelen, R., Bellander, T., Cesaroni, G., Cirach, M.,
 471 Cyrys, J., de Hoogh, K., De Nazelle, A., de Vocht, F., Declercq, C., Dèdelè, A., Eriksen, K., Galassi, C.,
 472 Gražulevičienė, R., Grivas, G., Heinrich, J., Hoffmann, B., Iakovides, M., Ineichen, A., Katsouyanni, K.,
 473 Korek, M., Krämer, U., Kuhlbusch, T., Lanki, T., Madsen, C., Meliefste, K., Mölter, A., Mosler, G.,
 474 Nieuwenhuijsen, M., Oldenwening, M., Pennanen, A., Probst-Hensch, N., Quass, U., Raaschou-Nielsen,

475 O., Ranzi, A., Stephanou, E., Sugiri, D., Udvardy, O., Vaskövi, É., Weinmayr, G., Brunekreef, B., and
 476 Hoek, G.: Spatial variation of PM_{2.5}, PM₁₀, PM_{2.5} absorbance and PM_{coarse} concentrations between and
 477 within 20 European study areas and the relationship with NO₂ – Results of the ESCAPE project, *Atmos.*
 478 *Environ.*, 62, 303–317, <https://doi.org/10.1016/j.atmosenv.2012.08.038>, 2012.

479 El-Hamouz, A.: Effect of Surfactant Concentration and Operating Temperature on the Drop Size
 480 Distribution of Silicon Oil Water Dispersion, *J. Dispers. Sci. Technol.*, 28, 797–804,
 481 <https://doi.org/10.1080/01932690701345893>, 2007.

482 Evich, M. G., Davis, M. J. B., McCord, J. P., Acrey, B., Awkerman, J. A., Knappe, D. R. U., Lindstrom,
 483 A. B., Speth, T. F., Tebes-Stevens, C., Strynar, M. J., Wang, Z., Weber, E. J., Henderson, W. M., and
 484 Washington, J. W.: Per- and polyfluoroalkyl substances in the environment, *Science* (80-.), 375,
 485 <https://doi.org/10.1126/science.abg9065>, 2022.

486 Facchini, M. C., Mircea, M., Fuzzi, S., and Charlson, R. J.: Cloud albedo enhancement by surface-active
 487 organic solutes in growing droplets, *Nature*, 401, 257–259, <https://doi.org/10.1038/45758>, 1999.

488 Facchini, M. C., Decesari, S., Mircea, M., Fuzzi, S., and Loglio, G.: Surface tension of atmospheric wet
 489 aerosol and cloud/fog droplets in relation to their organic carbon content and chemical composition,
 490 *Atmos. Environ.*, 34, 4853–4857, [https://doi.org/10.1016/S1352-2310\(00\)00237-5](https://doi.org/10.1016/S1352-2310(00)00237-5), 2000.

491 Fan, W., Salmond, J. A., Dirks, K. N., Cabedo Sanz, P., Miskelly, G. M., and Rindelaub, J. D.: Evidence
 492 and Mass Quantification of Atmospheric Microplastics in a Coastal New Zealand City, *Environ. Sci.*
 493 *Technol.*, 56, 17556–17568, <https://doi.org/10.1021/acs.est.2c05850>, 2022.

494 Faust, J. A.: PFAS on atmospheric aerosol particles: a review, *Environ. Sci. Process. Impacts*, 25, 133–
 495 150, <https://doi.org/10.1039/D2EM00002D>, 2023.

496 Fraga, A. K., Santos, R. F., and Mansur, C. R. E.: Evaluation of the efficiency of silicone polyether
 497 additives as antifoams in crude oil, *J. Appl. Polym. Sci.*, 124, 4149–4156,

498 <https://doi.org/10.1002/app.35394>, 2012.

499 Gaines, G. L.: Surface tension of polymer solutions. I. Solutions of poly(dimethylsiloxanes), *J. Phys.*
500 *Chem.*, 73, 3143–3150, <https://doi.org/10.1021/j100843a060>, 1969.

501 Gérard, V., Nozière, B., Baduel, C., Fine, L., Frossard, A. A., and Cohen, R. C.: Anionic, Cationic, and
502 Nonionic Surfactants in Atmospheric Aerosols from the Baltic Coast at Askö, Sweden: Implications for
503 Cloud Droplet Activation, *Environ. Sci. Technol.*, 50, 2974–2982,
504 <https://doi.org/10.1021/acs.est.5b05809>, 2016.

505 Ghorbanizadeh, S. and Rostami, B.: Surface and Interfacial Tension Behavior of Salt Water Containing
506 Dissolved Amphiphilic Compounds of Crude Oil: The Role of Single-Salt Ionic Composition, *Energy &*
507 *Fuels*, 31, 9117–9124, <https://doi.org/10.1021/acs.energyfuels.7b01394>, 2017.

508 Goebel, A. and Lunkenheimer, K.: Interfacial Tension of the Water/ n -Alkane Interface, *Langmuir*, 13,
509 369–372, <https://doi.org/10.1021/la960800g>, 1997.

510 Goßmann, I., Herzke, D., Held, A., Schulz, J., Nikiforov, V., Georgi, C., Evangeliou, N., Eckhardt, S.,
511 Gerdt, G., Wurl, O., and Scholz-Böttcher, B. M.: Occurrence and backtracking of microplastic mass
512 loads including tire wear particles in northern Atlantic air, *Nat. Commun.*, 14, 3707,
513 <https://doi.org/10.1038/s41467-023-39340-5>, 2023.

514 Harkins, W. D.: *The physical chemistry of surface films*, Reinhold, 1952.

515 Hitzenberger, R., Berner, A., Kasper-Giebl, A., Löflund, M., and Puxbaum, H.: Surface tension of Rax
516 cloud water and its relation to the concentration of organic material, *J. Geophys. Res. Atmos.*, 107, 1–6,
517 <https://doi.org/10.1029/2002JD002506>, 2002.

518 Holzinger, R.: PTRwid: A new widget tool for processing PTR-TOF-MS data, *Atmos. Meas. Tech.*, 8,
519 3903–3922, <https://doi.org/10.5194/amt-8-3903-2015>, 2015.

520 Ivleva, N. P.: *Chemical Analysis of Microplastics and Nanoplastics: Challenges, Advanced Methods, and*

521 Perspectives, *Chem. Rev.*, 121, 11886–11936, <https://doi.org/10.1021/acs.chemrev.1c00178>, 2021.
 522 Kanellopoulos, A. G. and Owen, M. J.: Adsorption of sodium dodecyl sulphate at the silicone fluid/water
 523 interface, *Trans. Faraday Soc.*, 67, 3127, <https://doi.org/10.1039/tf9716703127>, 1971.
 524 Kirchsteiger, B., Materić, D., Happenhofer, F., Holzinger, R., and Kasper-Giebl, A.: Fine micro- and
 525 nanoplastics particles (PM_{2.5}) in urban air and their relation to polycyclic aromatic hydrocarbons, *Atmos.*
 526 *Environ.*, 301, <https://doi.org/10.1016/j.atmosenv.2023.119670>, 2023.
 527 Koelmans, A. A., Redondo-Hasselerharm, P. E., Mohamed Nor, N. H., and Kooi, M.: Solving the
 528 Nonalignment of Methods and Approaches Used in Microplastic Research to Consistently Characterize
 529 Risk, *Environ. Sci. Technol.*, 54, 12307–12315, <https://doi.org/10.1021/acs.est.0c02982>, 2020.
 530 Koelmans, A. A., Redondo-Hasselerharm, P. E., Nor, N. H. M., de Ruijter, V. N., Mintenig, S. M., and
 531 Kooi, M.: Risk assessment of microplastic particles, *Nat. Rev. Mater.*, 7, 138–152,
 532 <https://doi.org/10.1038/s41578-021-00411-y>, 2022.
 533 Kooi, M. and Koelmans, A. A.: Simplifying Microplastic via Continuous Probability Distributions for
 534 Size, Shape, and Density, *Environ. Sci. Technol. Lett.*, 6, 551–557,
 535 <https://doi.org/10.1021/acs.estlett.9b00379>, 2019.
 536 Lee, H. D. and Tivanski, A. V.: Atomic Force Microscopy: An Emerging Tool in Measuring the Phase
 537 State and Surface Tension of Individual Aerosol Particles, *Annu. Rev. Phys. Chem.*, 72, 235–252,
 538 <https://doi.org/10.1146/annurev-physchem-090419-110133>, 2021.
 539 Li, Y., Shao, L., Wang, W., Zhang, M., Feng, X., Li, W., and Zhang, D.: Airborne fiber particles: Types,
 540 size and concentration observed in Beijing, *Sci. Total Environ.*, 705, 135967,
 541 <https://doi.org/10.1016/j.scitotenv.2019.135967>, 2020.
 542 Luo, P., Bai, M., He, Q., Peng, Z., Wang, L., Dong, C., Qi, Z., Zhang, W., Zhang, Y., and Cai, Z.: A
 543 Novel Strategy to Directly Quantify Polyethylene Microplastics in PM 2.5 Based on Pyrolysis-Gas

544 Chromatography–Tandem Mass Spectrometry, *Anal. Chem.*, 95, 3556–3562,
545 <https://doi.org/10.1021/acs.analchem.2c05477>, 2023.

546 Mircea, M., Facchini, M. C., Decesari, S., Cavalli, F., Emblico, L., Fuzzi, S., Vestin, A., Rissler, J.,
547 Swietlicki, E., Frank, G., Andreae, M. O., Maenhaut, W., Rudich, Y., and Artaxo, P.: Importance of the
548 organic aerosol fraction for modeling aerosol hygroscopic growth and activation: a case study in the
549 Amazon Basin, *Atmos. Chem. Phys.*, 5, 3111–3126, <https://doi.org/10.5194/acp-5-3111-2005>, 2005.

550 Mitrano, D. M., Wick, P., and Nowack, B.: Placing nanoplastics in the context of global plastic pollution,
551 *Nat. Nanotechnol.*, 16, 491–500, <https://doi.org/10.1038/s41565-021-00888-2>, 2021.

552 Mizuguchi, H., Takeda, H., Kinoshita, K., Takeuchi, M., Takayanagi, T., Teramae, N., Pipkin, W.,
553 Matsui, K., Watanabe, A., and Watanabe, C.: Direct analysis of airborne microplastics collected on quartz
554 filters by pyrolysis-gas chromatography/mass spectrometry, *J. Anal. Appl. Pyrolysis*, 171, 105946,
555 <https://doi.org/10.1016/j.jaap.2023.105946>, 2023.

556 Mohamed Nor, N. H., Kooi, M., Diepens, N. J., and Koelmans, A. A.: Lifetime Accumulation of
557 Microplastic in Children and Adults, *Environ. Sci. Technol.*, 55, 5084–5096,
558 <https://doi.org/10.1021/acs.est.0c07384>, 2021.

559 Nowak, E., Kovalchuk, N. M., Che, Z., and Simmons, M. J. H.: Effect of surfactant concentration and
560 viscosity of outer phase during the coalescence of a surfactant-laden drop with a surfactant-free drop,
561 *Colloids Surfaces A Physicochem. Eng. Asp.*, 505, 124–131,
562 <https://doi.org/10.1016/j.colsurfa.2016.02.016>, 2016.

563 Ovadnevaite, J., Zuend, A., Laaksonen, A., Sanchez, K. J., Roberts, G., Ceburnis, D., Decesari, S.,
564 Rinaldi, M., Hodas, N., Facchini, M. C., Seinfeld, J. H., and O’ Dowd, C.: Surface tension prevails over
565 solute effect in organic-influenced cloud droplet activation, *Nature*, 546, 637–641,
566 <https://doi.org/10.1038/nature22806>, 2017.

567 Peñalver, R., Costa-Gómez, I., Arroyo-Manzanares, N., Moreno, J. M., López-García, I., Moreno-Grau,
568 S., and Córdoba, M. H.: Assessing the level of airborne polystyrene microplastics using
569 thermogravimetry-mass spectrometry: Results for an agricultural area, *Sci. Total Environ.*, 787, 147656,
570 <https://doi.org/10.1016/j.scitotenv.2021.147656>, 2021.

571 Petters, M. D. and Kreidenweis, S. M.: A single parameter representation of hygroscopic growth and
572 cloud condensation nucleus activity, *Atmos. Chem. Phys.*, 7, 1961–1971, [https://doi.org/10.5194/acp-7-](https://doi.org/10.5194/acp-7-1961-2007)
573 1961-2007, 2007.

574 Picó, Y. and Barceló, D.: Pyrolysis gas chromatography-mass spectrometry in environmental analysis:
575 Focus on organic matter and microplastics, *TrAC Trends Anal. Chem.*, 130, 115964,
576 <https://doi.org/10.1016/j.trac.2020.115964>, 2020.

577 Putaud, J.-P., Van Dingenen, R., Alastuey, A., Bauer, H., Birmili, W., Cyrys, J., Flentje, H., Fuzzi, S.,
578 Gehrig, R., Hansson, H. C., Harrison, R. M., Herrmann, H., Hitenberger, R., Hüglin, C., Jones, A. M.,
579 Kasper-Giebl, A., Kiss, G., Kousa, A., Kuhlbusch, T. A. J., Löschau, G., Maenhaut, W., Molnar, A.,
580 Moreno, T., Pekkanen, J., Perrino, C., Pitz, M., Puxbaum, H., Querol, X., Rodriguez, S., Salma, I.,
581 Schwarz, J., Smolik, J., Schneider, J., Spindler, G., ten Brink, H., Tursic, J., Viana, M., Wiedensohler, A.,
582 and Raes, F.: A European aerosol phenomenology – 3: Physical and chemical characteristics of particulate
583 matter from 60 rural, urban, and kerbside sites across Europe, *Atmos. Environ.*, 44, 1308–1320,
584 <https://doi.org/10.1016/j.atmosenv.2009.12.011>, 2010.

585 Querol, X., Alastuey, A., Moreno, T., Viana, M. M., Castillo, S., Pey, J., Rodríguez, S., Artiñano, B.,
586 Salvador, P., Sánchez, M., García Dos Santos, S., Herce Garraleta, M. D., Fernandez-Patier, R., Moreno-
587 Grau, S., Negral, L., Minguillón, M. C., Monfort, E., Sanz, M. J., Palomo-Marín, R., Pinilla-Gil, E.,
588 Cuevas, E., de la Rosa, J., and Sánchez de la Campa, A.: Spatial and temporal variations in airborne
589 particulate matter (PM₁₀ and PM_{2.5}) across Spain 1999–2005, *Atmos. Environ.*, 42, 3964–3979,
590 <https://doi.org/10.1016/j.atmosenv.2006.10.071>, 2008.

591 Revell, L. E., Kuma, P., Le Ru, E. C., Somerville, W. R. C., and Gaw, S.: Direct radiative effects of
 592 airborne microplastics, *Nature*, 598, 462–467, <https://doi.org/10.1038/s41586-021-03864-x>, 2021.

593 Rosenfeld, D., Andreae, M. O., Asmi, A., Chin, M., de Leeuw, G., Donovan, D. P., Kahn, R., Kinne, S.,
 594 Kivekäs, N., Kulmala, M., Lau, W., Schmidt, K. S., Suni, T., Wagner, T., Wild, M., and Quaas, J.: Global
 595 observations of aerosol-cloud-precipitation-climate interactions, *Rev. Geophys.*, 52, 750–808,
 596 <https://doi.org/10.1002/2013RG000441>, 2014.

597 Ruehl, C. R., Chuang, P. Y., Nenes, A., Cappa, C. D., Kolesar, K. R., and Goldstein, A. H.: Strong
 598 evidence of surface tension reduction in microscopic aqueous droplets, *Geophys. Res. Lett.*, 39, n/a-n/a,
 599 <https://doi.org/10.1029/2012GL053706>, 2012.

600 Ruehl, C. R., Davies, J. F., and Wilson, K. R.: An interfacial mechanism for cloud droplet formation on
 601 organic aerosols, *Science (80-.)*, 351, 1447–1450, <https://doi.org/10.1126/science.aad4889>, 2016.

602 Sheng, X., Lai, Y., Yu, S., Li, Q., Zhou, Q., and Liu, J.: Quantitation of Atmospheric Suspended
 603 Polystyrene Nanoplastics by Active Sampling Prior to Pyrolysis–Gas Chromatography–Mass
 604 Spectrometry, *Environ. Sci. Technol.*, 57, 10754–10762, <https://doi.org/10.1021/acs.est.3c02299>, 2023.

605 Soloviev, A. V., Haus, B. K., McGauley, M. G., Dean, C. W., Ortiz-Suslow, D. G., Laxague, N. J. M.,
 606 and Özgökmen, T. M.: Surface dynamics of crude and weathered oil in the presence of dispersants:
 607 Laboratory experiment and numerical simulation, *J. Geophys. Res. Ocean.*, 121, 3502–3516,
 608 <https://doi.org/10.1002/2015JC011533>, 2016.

609 Stein, A. F., Draxler, R. R., Rolph, G. D., Stunder, B. J. B., Cohen, M. D., and Ngan, F.: NOAA’s
 610 HYSPLIT Atmospheric Transport and Dispersion Modeling System, *Bull. Am. Meteorol. Soc.*, 96, 2059–
 611 2077, <https://doi.org/10.1175/BAMS-D-14-00110.1>, 2015.

612 Stifelman, M.: Using doubly-labeled water measurements of human energy expenditure to estimate
 613 inhalation rates, *Sci. Total Environ.*, 373, 585–590, <https://doi.org/10.1016/j.scitotenv.2006.11.041>, 2007.

614 Velimirovic, M., Tirez, K., Verstraelen, S., Frijns, E., Remy, S., Koppen, G., Rotander, A., Bolea-
 615 Fernandez, E., and Vanhaecke, F.: Mass spectrometry as a powerful analytical tool for the characterization
 616 of indoor airborne microplastics and nanoplastics, *J. Anal. At. Spectrom.*, 36, 695–705,
 617 <https://doi.org/10.1039/d1ja00036e>, 2021a.

618 Velimirovic, M., Tirez, K., Verstraelen, S., Frijns, E., Remy, S., Koppen, G., Rotander, A., Bolea-
 619 Fernandez, E., and Vanhaecke, F.: Mass spectrometry as a powerful analytical tool for the characterization
 620 of indoor airborne microplastics and nanoplastics, *J. Anal. At. Spectrom.*, 36, 695–705,
 621 <https://doi.org/10.1039/d1ja00036e>, 2021b.

622 Vudayagiri, S., Junker, M. D., and Skov, A. L.: Factors affecting the surface and release properties of thin
 623 polydimethylsiloxane films, *Polym. J.*, 45, 871–878, <https://doi.org/10.1038/pj.2012.227>, 2013.

624 Winoto, Loahardjo, N., Takamura, K., and Morrow, N. R.: Spreading and Retraction of Spilled Crude Oil
 625 on Seawater, *Int. Oil Spill Conf. Proc.*, 2014, 1465–1473, [https://doi.org/10.7901/2169-3358-](https://doi.org/10.7901/2169-3358-2014.1.1465)
 626 [2014.1.1465](https://doi.org/10.7901/2169-3358-2014.1.1465), 2014.

627 Worton, D. R., Moreno, S., O’Daly, K., and Holzinger, R.: Development of an International System of
 628 Units (SI)-traceable transmission curve reference material to improve the quantitation and comparability
 629 of proton-transfer-reaction mass-spectrometry measurements, *Atmos. Meas. Tech.*, 16, 1061–1072,
 630 <https://doi.org/10.5194/amt-16-1061-2023>, 2023.

631 Xu, J.-L., Thomas, K. V., Luo, Z., and Gowen, A. A.: FTIR and Raman imaging for microplastics
 632 analysis: State of the art, challenges and prospects, *TrAC Trends Anal. Chem.*, 119, 115629,
 633 <https://doi.org/10.1016/j.trac.2019.115629>, 2019.

634 Yao, P., Chianese, E., Kairys, N., Holzinger, R., Materić, D., Sirignano, C., Riccio, A., Ni, H., Huang,
 635 R.-J., and Dusek, U.: A large contribution of methylsiloxanes to particulate matter from ship emissions,
 636 *Environ. Int.*, 165, 107324, <https://doi.org/10.1016/j.envint.2022.107324>, 2022.

637 Yao, P., Holzinger, R., Materić, D., Oyama, B. S., de Fátima Andrade, M., Paul, D., Ni, H., Noto, H.,
638 Huang, R.-J., and Dusek, U.: Methylsiloxanes from Vehicle Emissions Detected in Aerosol Particles,
639 Environ. Sci. Technol., 57, 14269–14279, <https://doi.org/10.1021/acs.est.3c03797>, 2023.

640 Zeppieri, S., Rodríguez, J., and López de Ramos, A. L.: Interfacial Tension of Alkane + Water Systems,
641 J. Chem. Eng. Data, 46, 1086–1088, <https://doi.org/10.1021/je000245r>, 2001.

642 Zheng, Y., Li, J., Sun, C., Cao, W., Wang, M., Jiang, F., and Ju, P.: Comparative study of three sampling
643 methods for microplastics analysis in seawater, Sci. Total Environ., 765, 144495,
644 <https://doi.org/10.1016/j.scitotenv.2020.144495>, 2021.

645 Zhou, X., Cao, Z., Ma, Y., Wang, L., Wu, R., and Wang, W.: Concentrations, correlations and chemical
646 species of PM_{2.5}/PM₁₀ based on published data in China: Potential implications for the revised particulate
647 standard, Chemosphere, 144, 518–526, <https://doi.org/10.1016/j.chemosphere.2015.09.003>, 2016.

648